 doi:10.20944/preprints202206.0399.v1

Article

Theoretical Perspectives on the Gas-phase Oxidation Mechanism and Kinetics of Carbazole Initiated by OH Radical in the Atmosphere

Zhuochao Teng[1], Xiaotong Wang[1], Mohammad Hassan Hadizadeh[1], Yanan Han[1], Xianwei Zhao[1], Qi Zhang[1], Hetong Wang[1], Ying Li[1], Fei Xu[1]* and Yanhui Sun[2]

[1] Environment Research Institute, Shandong University, Qingdao 266237, P. R. China.
[2] College of Environment and Safety Engineering, Qingdao University of Science & Technology, Qingdao 266042, P. R. China.
* Corresponding authors: E-mail: xufei@sdu.edu.cn; Fax: 86-532-5863 1986.

Abstract: Carbazole is one of the typical heterocyclic aromatic compounds (NSO-HETs) observed in polluted urban atmosphere, which has become a serious environmental concern. The most important atmospheric loss process of carbazole is the reaction with OH radical. The present work investigated the mechanism of OH-initiated atmospheric oxidation degradation of carbazole by using density functional theory (DFT) calculations at the M06-2X/6-311++G(3df,2p)//M06-2X/6-311+G(d,p) level. The rate constants were determined by the Rice-Ramsperger-Kassel-Marcus (RRKM) theory. The lifetime of carbazole determined by OH was compared with other typical NSO-HETs. The theoretical results show that the degradation of carbazole initiated by OH radical includes four types of reactions: OH additions to "bend" C atoms, OH additions to "benzene ring" C atoms, H abstractions from C-H bonds and the H abstraction from N-H bond. The OH addition to C1 atom and the H abstraction from N-H bond are energetically favorable. The main oxidation products are hydroxycarbazole, dialdehyde, carbazolequinone, carbazole-ol, hydroxy-carbazole-one and hydroperoxyl-carbazole-one. The calculated overall rate constant of carbazole oxidation by OH radical is 6.52×10^{-12} cm^3 $molecule^{-1}$ s^{-1} and the atmospheric lifetime is 43.92 h under the condition of 298 K and 1 atm. The lifetime of carbazole determined by OH radical is similar with that of dibenzothiophene oxidation but longer than those of pyrrole, indole, dibenzofuran and fluorene. This work provides a better understanding of the reactivity of carbazole in the atmospheric environment, the formation of secondary organic aerosols, and the chemical degradation and removal of carbazole in the atmospheric environment.

Keywords: carbazole; OH radical; rate constants; oxidation mechanism; density functional theory (DFT)

1. Introduction

Heterocyclic aromatic compounds (NSO-HETs) are important contaminants characterized by the presence of fused aromatic rings, which pose a great threat to the environment and human health due to their genotoxicity, mutagenesis potential and carcinogenicity [1–4]. Carbazole, one of a typical nitrogen substituted NSO-HETs, has been extensively applied in pesticides, dyes, lubricants, detergents and pharmaceutical manufacturing [5,6]. The main sources of carbazole include waste incineration [7], biomass burning [8], tobacco smoke [9], synthetic dye production [10], aluminum manufacturing and rubber [11], and oil and coal burning [12]. Carbazole can be considered as a one-nitrogen-substituted dibenzofuran, which exhibits mutagenicity, toxicity and adverse effect on humans. Therefore, it can be viewed as dioxin-like compound and listed as the second-class carcinogen of the World Health Organization [9,13,14]. Given these harmful consequences, obtaining detailed insight into the degradation of carbazole in the atmosphere

 doi:10.20944/preprints202206.0399.v1

will deepen our understanding of the degradation mechanisms of dioxin-like compounds and could lead to emission-reduction and dioxin-control strategies.

At present, carbazole has been constantly detected in atmospheric samples, river sediments, groundwater and contaminated sites [5]. In the atmosphere, carbazole can cause the formation of nitrogen oxides by burning, which can accelerate the formation of acid rain and the destruction of ozone layer [15,16]. The measurement by Esen et al. in Bursa showed that the average gas and particle phase concentrations of carbazole were 7.6 ± 9.9, 1.1 ± 1.2, 3.3 ± 5.0 and 1.2 ± 0.7 ng/m^3 in residential, traffic, industrial and campus area, respectively [5]. Air samples collected from coal burned indoors showed that the maximum concentration of carbazole in the air was up to 7,500-20,168 ng/m^3 [3,9]. Heim et al. measured the concentration of carbazole in an undisturbed sediment core collected from the Lippe River in Germany, ranging from 11 to 172 ng/g [17]. Carbazole can undergo diverse chemical reactions and long-distance transport in the atmosphere, which may induce more complex contamination in remote sites.

In the troposphere, carbazole can be removed by dry and wet subsidence as well as photochemical reactions, and the main sinks are the oxidation reactions with major oxidants such as OH radical, NO_3 radical and O_3. Among these oxidants, OH radical [18] accounts for a quite high proportion in determining the oxidation power of the atmosphere, especially in the daytime [19]. Reaction with OH radical is considered to be the main chemical process for carbazole in the atmosphere [20]. Therefore, it is necessary to investigate the reaction mechanism of carbazole with OH radical to clarify its atmospheric transformations. To date, only one study had been conducted to remove carbazole initiated by OH radical [21]. The reaction mechanism has not been fully elucidated. Clearly, more study is needed to obtain more comprehensive knowledge of the carbazole oxidation by OH radical.

Due to the lack of efficient detection schemes for intermediate radical species, a full analysis of the atmospheric processes of the reaction mechanism of OH-initiated atmospheric oxidation of carbazole is limited in the laboratory studies, which hinders to further evaluate the atmospheric effect of carbazole. Therefore, in this paper, with the aid of the density functional theory (DFT) method, a comprehensive degradation mechanism of carbazole initiated by OH radical in the presence of O_2 and NO was carried out. The main products and reaction pathways were determined. Additionally, the rate constants for the vital reactions of carbazole degradation by OH radical were calculated by RRKM theory and the lifetimes were evaluated [22,23]. The obtained rate constants and lifetime were compared with the literature values of other NSO-HETs (pyrrole/indole/dibenzothiophene/dibenzofuran/fluorine) degradation by OH radical [24-29]. The influences of steric structure and element substitution and of NSO-HETs on the lifetimes were discussed. This work provides a theoretical investigation of the oxygenated mechanism of NSO-HETs in the atmosphere and should help to clarify their potential health risk for determining the reaction pathways and atmospheric influence of carbazole.

2. Computational detail

2.1. Thermodynamic calculation

All the calculations on the geometries, energies and frequencies for reactants, complexes, transition states and products were determined using the Gaussian 09 program package [30]. Geometrical optimizations and vibrational frequency calculations were carried out using M06-2X functional method with 6-311+G(d,p) basis set [31]. The vibrational frequency calculations were used to determine the nature of each species and provide the zero-point energy (ZPE) values. Transition states have exactly one imaginary frequency, whereas reactants, intermediates and products have real frequencies. The minimum energy path (MEP) was obtained by the IRC calculation to confirm the connections between transition states and the corresponding energy minima along the reaction path [32]. In order to obtain more reliable energy results, based on the geometries obtained at 6-311+G(d,p) level, the single-point energies were calculated by using the more accurate

Preprints (www.preprints.org) | NOT PEER-REVIEWED | Posted: 29 June 2022 doi:10.20944/preprints202206.0399.v1

basis set 6-311++G(3df,2p). The potential barriers are the energy differences between transition states and reactants, and the reaction enthalpies are the energy differences between products and reactants. All the relative energies were quoted and discussed in this paper include ZPE corrections.The structures of CTP-H_2O complexes along with the structure of TPh-H2O are presented in Figure 1 and Figure S1. Among the 19 hydrated CTPs, due to the different ortho-substitution pattern of hydrated TPh, hydrated CTPs contain three kind of congeners: hydrated CTPs with two ortho-chlorine substituents (2,6-DCTP-H_2O, 2,3,6-TCTP-H_2O, 2,4,6-TCTP-H_2O, 2,3,4,6-TeCTP-H_2O, 2,3,5,6-TeCTP-H_2O, and PCTP-H_2O), hydrated CTPs with two ortho-hydrogen substituents (3-CTP-H_2O, 4-CTP-H_2O, 3,4-DCTP-H_2O, 3,5-DCTP-H_2O, and 3,4,5-TCTP-H_2O) and hydrated CTPs with one ortho-chlorine substituent and one ortho-hydrogen substituent (2-CTP-H_2O, 2,3-DCTP-H_2O, 2,4-DCTP-H_2O, 2,5-DCTP-H_2O, 2,3,4-TCTP-H_2O, 2,3,5-TCTP-H_2O, 2,4,5-TCTP-H_2O, and 2,3,4,5-TeCTP-H_2O). In particular, CTP-H_2O complexes with one ortho-hydrogen atom have two conformers. The conformer with the sulfhydryl-hydrogen pointing toward the closest neighboring Cl is labeled as the syn-conformer and otherwise the anti-conformer (Figure 2). For a given CTP-H_2O complex, the syn-conformer is about 0.7 kcal mol^{-1} more stable than the corresponding anti-form, suggesting a stabilization effect because of intramolecular hydrogen bonding. So, throughout this paper, CTP-H_2O complexes denote the syn-conformers.

2.2. Kinetic calculation

Rice-Ramsperger-Kassel-Marcus (RRKM) theory [22,23]. was carried out to calculate rate constants of the crucial elementary reactions discussed in the present work by means of the MESMER program [33]. The RRKM rate constant is given by:

$$k(E) = \frac{W(E)}{h\rho(E)} \tag{1}$$

where, W(E) is the rovibrational sum of states at the transition state, ρ(E) is the density of states of reactants, and h is Planck's constant. Then, the canonical rate constant k(T) is determined from the usual equation:

$$k(T) = \frac{1}{Q(T)}\int k(E)\rho(E)\exp(-\beta E)dE \tag{2}$$

where, Q(T) is the reactant partition function, k(E) is the rate constant in a microcanonical ensemble with energy E, $\beta = 1/(k_B T)$, and k_B is Boltzmann's constant. The collisional parameters are estimated according to Gilbert and Smith [34].The bath gas is set as nitrogen. The default pressure is 1 atm and the temperature is 298 K. The exponential-down model is assumed for the collisional energy transfer with $<\triangle E_{down}>$ of 250/cm.

3. Results and discussion

The reliability and accuracy of the M06-2X/6-31+G(d,p) level for the geometry parameters of carbazole have been compared with experimental and other calculated values are listed in Table S1 of Supplementary data [35,36]. The optimized geometries of carbazole at the M06-2X/6-31+G(d,p) level are in reasonable accordance with the corresponding experimental values, and the largest discrepancy remains within 4.5% and 2.3% for the bond lengths and bond angles, respectively, except two abnormal values [36]. The optimized geometries of carbazole at the M06-2X/6-31+G(d,p) level match better with the calculated values on the MP2/6-31G* level and the largest discrepancy remains within 0.5% for both bond lengths and bond angles. Typical transition states involved in the degradation of carbazole initiated by OH radical are shown in Fig. 8. Imaginary frequencies, zero-point energies, total energies and cartesian coordinates for the transition states involved in the oxidation reaction of carbazole initiated by OH radical are depicted in Table S3 and Table S5 of Supplementary data.

Preprints (www.preprints.org) | NOT PEER-REVIEWED | Posted: 29 June 2022 doi:10.20944/preprints202206.0399.v1

3.1. Reaction of carbazole and OH radical

The molecular structures of carbazole are depicted in Fig. 1, from which the C atoms in carbazole are numbered. There are C-H, N-H and C=H bonds in carbazole. Thus, the reaction pathways of carbazole with OH include H abstractions from C-H or N-H bonds and OH additions on C=C bonds. The OH addition and H abstraction scheme of carbazole embedded with the potential barriers ΔE (in kcal/mol) and reaction heats ΔH (in kcal/mol, 0 K) are presented in Fig. 1.

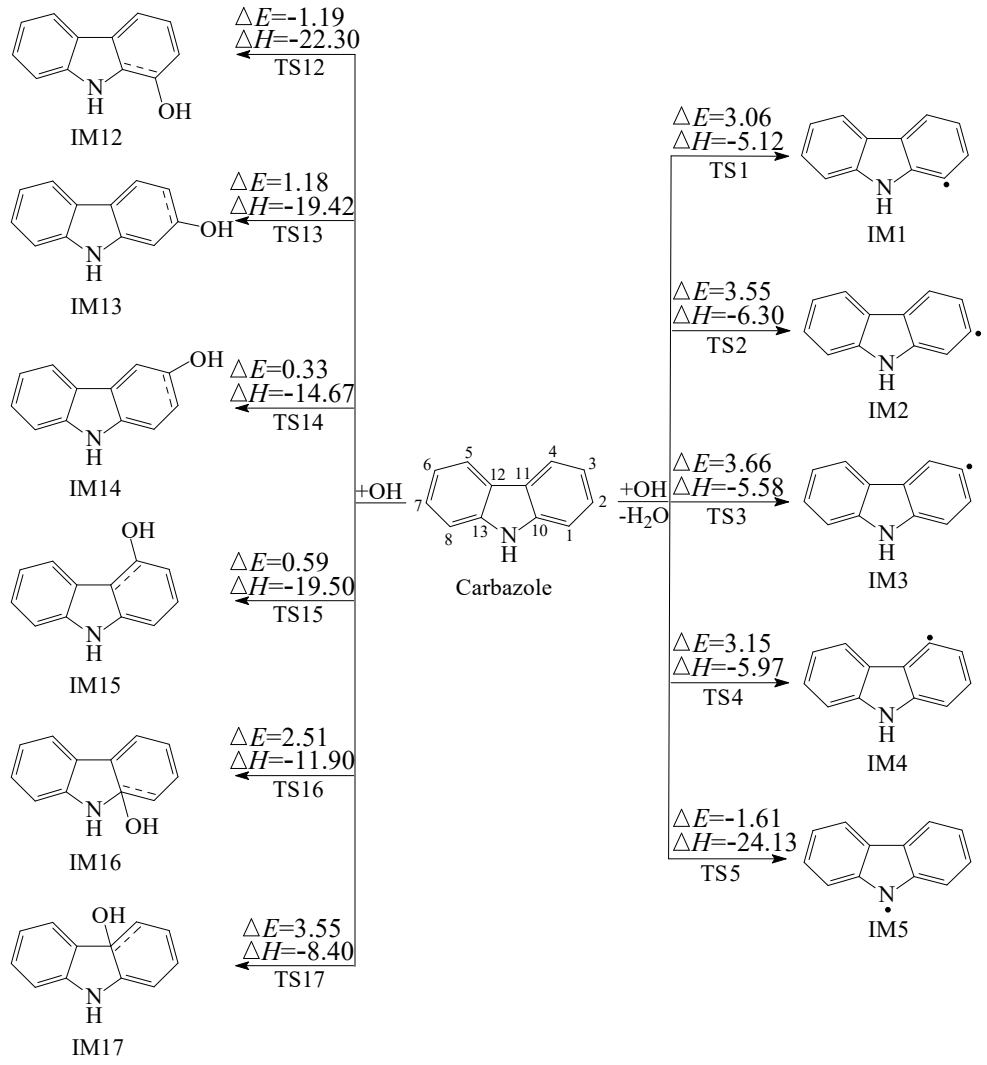

Figure 1. The OH addition and H abstraction reaction scheme of carbazole embedded with the potential barriers ΔE (in kcal/mol) and reaction heats ΔH (in kcal/mol, 0 K).

Nine H abstraction pathways of carbazole initiated by OH radical were identified: one H abstraction from the N-H and eight H abstractions from the C-H in benzene rings (C1-H, C2-H, C3-H, C4-H, C5-H, C6-H, C7-H and C8-H bonds). Owning to carbazole molecule belongs to the C_{2v} symmetrical structure, C1 and C8, C2 and C7, C3 and C6, and C4 and C5 are equivalent. Therefore, only one benzene ring of carbazole is discussed. As shown in Fig. 1, at the M06-2X/6-311++G(3df,2p)//M06-2X/6-311+G(d,p) level, all the four C-H abstractions have the potential barriers in the range from 3.06 to 3.66 kcal/mol, and are exothermic by −5.12 ~ −6.30 kcal/mol. The H abstraction from the N-H bond is barrierless, and is exothermic by 24.13 kcal/mol, which is more favorable than those from C-H bonds. Thus, in the abstraction reactions, the N-H abstraction is the most favorable reaction pathway, resulting in the formation of intermediate IM5. Only the subsequent reactions of IM5 intermediate are further discussed.

Preprints (www.preprints.org) | NOT PEER-REVIEWED | Posted: 29 June 2022 doi:10.20944/preprints202206.0399.v1

OH radical can also attack C=C unsaturated bonds and add to the C atoms in benzene ring of carbazole molecule. C10, C11, C12 and C13 are inside the "bend" of the carbazole molecule, which can be called the "bend" C atoms. C1, C2, C3, C4, C5, C6, C7 and C8 are in the benzene ring and out of the "bend" of the carbazole molecule, which can be called the "benzene ring" C atoms. Considering the C_{2V} symmetry, six different OH-carbazole adduct isomers are labeled as IM12-IM17 in Fig. 1, which can be readily formed through the OH additions to the C1, C2, C3, C4, C10, and C11 atoms. In Fig. 1, the OH additions to "benzene ring" C atoms are highly exothermic (−22.30 ~ −14.67 kcal/mol) with low potential barriers (−1.19 ~ 1.18 kcal/mol). However, the potential barriers of OH additions to "bend" C atoms are 2.51 and 3.55 kcal/mol, which are higher than those to C1, C2, C3 and C4 atoms. In addition, OH additions to "bend" C atoms are less exothermic (−11.90 ~ −8.40 kcal/mol) than those to "bend" C atoms Thus, OH additions to "benzene ring" C atoms are energetically more favorable than the those to "bend" C atoms. The OH additions to these C9 and C10 atoms are sterically hindered and energetically unfavorable. In the "benzene ring" C atoms, the OH addition reaction to the C1 atom has the lowest potential barrier and is the most exothermic reaction among those to other C atoms, resulting in the formation of IM12. In Fig. 1, the H abstraction reaction from the N-H bond and OH addition to C1 atoms have similar potential barriers and reaction heats, which indicates the two reactions are competitive.

Comparison of the OH additions to "benzene ring" C atoms with the H abstractions from C-H bonds shows that the OH additions to "benzene ring" C atoms have lower potential barriers and higher heat releases than the H abstractions from C-H bonds. Thus, the OH additions to "benzene ring" C atoms are energetically more favorable than the H abstractions from C-H bonds. This agrees well with the experimental pattern that the reaction of aromatic compounds with OH is mainly through the OH addition to "benzene ring" C atoms (approximately 90 percent) rather than the H abstraction from C-H bonds, such as in the case of naphthalene [37], anthracene [38], and phenanthrene [39,40]. Hence, the H abstractions in benzene rings are not considered further in the subsequent reactions for the degradation of CA under the general atmospheric conditions.

3.2. Subsequent reaction

The intermediates produced by the abstraction and addition reactions of carbazole with OH radical contain unpaired electrons and can subsequently react with O_2/NO in the atmosphere.

3.2.1. Reactions with O_2

Fig. 2 shows the reaction pathways of carbazole-OH adducts (IM12-IM15) with O_2. Firstly, carbazole-OH adducts can react via a simple metathesis mechanism to yield hydroxycarbazoles and HO_2 radical through H abstractions from the C-H bonds. The potential barriers of these hydroxycarbazole formation processes are in the range of −33.66 ~ −29.03 kcal/mol. The processes are strongly exothermic by −68.78 ~ −62.43 kcal/mol. The overall reactions, carbazole + OH + O_2 → hydroxycarbazole + HO_2 have the total potential barriers of −33.33 ~ −27.84 kcal/mol, and are strongly exothermic by −86.02 ~ −83.45 kcal/mol. These indicate that the degradation pathways leading to the hydroxycarbazoles formation are easy to occur under the real atmospheric conditions. A comparison of the reaction pathways presented in Fig. 2 shows that the formation of 3-hydroxycarbazole (P4) from carbazole + OH + O_2 → hydroxycarbazole + HO_2 has the lowest total potential barriers of −33.33 kcal/mol and is energetically most favorable relative to the other H abstraction pathways, which means that 3-hydroxycarbazole is the main hydroxycarbazole product.

Preprints (www.preprints.org) | NOT PEER-REVIEWED | Posted: 29 June 2022 doi:10.20944/preprints202206.0399.v1

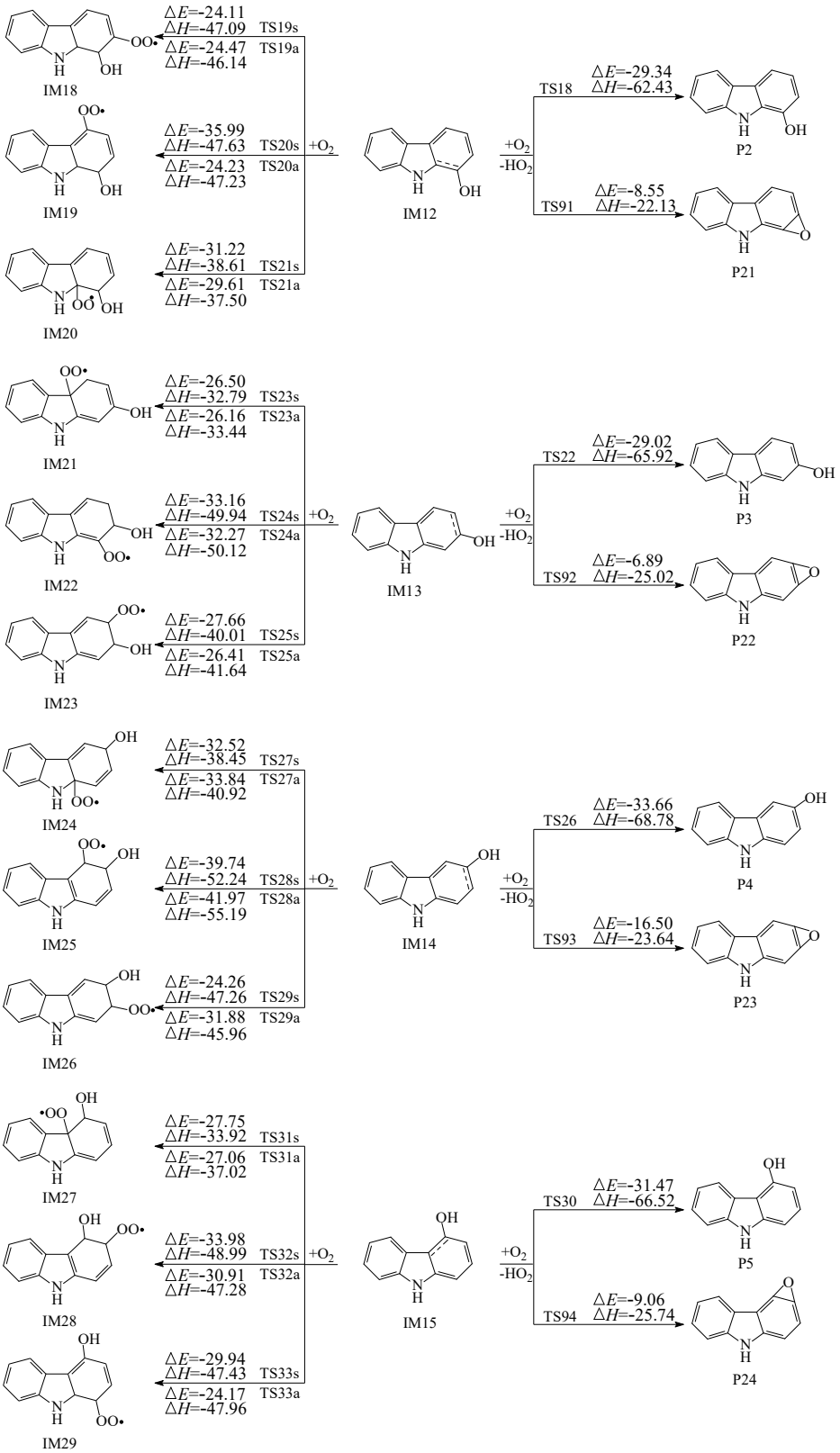

Figure 2. The O_2 addition and abstraction scheme of carbazole-OH adducts embedded with the potential barriers ΔE (in kcal/mol) and reaction heats ΔH (in kcal/mol, 0 K).

Secondly, carbazole-OH adducts may react with O_2 via H abstractions from the O-H bonds to produce carbazole-epoxides and HO_2 radical. As shown in Fig. 2, the carbazole-epoxide formations from the H abstractions of the O-H bonds have the potential barriers of −16.5 ~ −6.89 kcal/mol, which are higher than the hydroxycarbazole formations from

Preprints (www.preprints.org) | NOT PEER-REVIEWED | Posted: 29 June 2022 doi:10.20944/preprints202206.0399.v1

the H abstractions of the C-H bonds. In addition, the carbazole-epoxides formation from the H abstractions of the O-H bonds is exothermic by −25.74 ~ −22.13 kcal/mol, which is less than the hydroxycarbazoles formation from the H abstractions of the C-H bonds. This means that hydroxycarbazole formation is energetically more preferred than carbazole-epoxide formation, e.g. H abstraction from carbazole-OH with O_2 on the C-H bond is easier to occur than that on the O-H bond. This may be caused by the differences in bond length and bond energy between the C-H bond and the O-H bond in carbazole-OH intermediates. It can be seen from Table S2 that the bond energies of O-H bonds are 40.30 ~ 45.13 kcal/mol higher than those of C-H bonds and the bond lengths are about 0.14 angstrom shorter than the C-H bonds, which indicate that the break of C-H bonds is more favorable than that of O-H bonds.

Thirdly, O_2 can associate with the C atoms in the OH-carbazole adducts with an unpaired electron from two different directions: the anti- or syn-position with respect to the -OH group. Therefore, as depicted in Fig. 2, the O_2 addition reactions in the carbazole-OH adducts can form a series of carbazole-OH-O_2 adducts (namely IM18s/a-IM29s/a, where 's' denotes syn-position and 'a' denotes anti-position O_2 addition). The formation of carbazole-OH-O_2 adducts IM19, IM22, IM25 and IM28 from precursors IM12, IM13, IM14 and IM15 have lower potential barriers and are more exothermic compared to those of other O_2-OH-carbazole isomers. The potential barriers characterizing the formation of syn-position radicals are lower by 0.34 ~ 11.76 kcal/mol than those for the formation of anti-position O_2-OH-carbazole, except for IM18s/a, IM24s/a, IM25s/a and IM26s/a. In most cases, O_2 additions at syn-positions are energetically favored over those at anti-positions. Therefore, the formations of anti-isomers are of minor importance and will not be further discussed. In addition, considering IM12 is the most favored carbazole-OH adducts, the IM12-O_2 adducts (IM18s/a-IM20s/a) will be further discussed.

The scheme of reaction from the H abstraction product of carbazolide anion (IM5) with O_2 is depicted in Fig. 3. As shown in Fig. 3, O_2 may be added to the N atom of IM5 containing unpaired electrons to form OH-carbazole-O_2 adduct IM6. This process is barrierless and strongly exothermic.

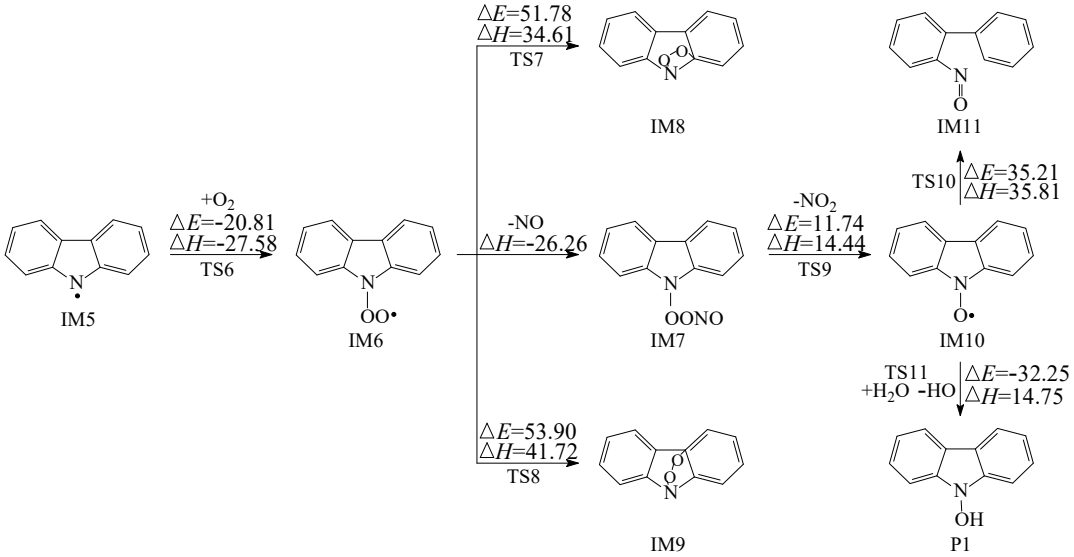

Figure 3. Syn- and anti- conformers of CTP and CTP-H_2O.

Fig. 2 and Fig. 3 show that the O_2 addition on N atom has a higher potential barrier and less heat release than those on C atoms of the benzene ring, which indicates that the O_2 addition on N atom is of minor importance than those on C atoms of benzene ring.

3.2.2. Subsequent reaction of carbazole-OH-O_2 intermediate

(1) Intramolecular H-transfer reaction

 doi:10.20944/preprints202206.0399.v1

As shown in Fig. 4, the intramolecular H transfer includes four modes: (1) H transfer from the -CH group to the -OO peroxyl group through four-membered ring transition state (H-transferCH4); (2) H transfer from the -CH group to the -OO peroxyl group through five-membered ring transition state (H-transferCH5); (3) H transfer from the O-H group to the -OO peroxyl group through six-membered ring transition state (H-transferOH); (4) H transfer from the -NH group to the -OO peroxyl group through five-membered ring transition state (H-transferNH).

Water molecules can participate in the H-transfer reactions. In TS40 and TS62, water molecules can reduce the potential barriers of the H-transferCH4, which means water molecules promote the H-transferCH4 reactions. In TS42, water molecule can increase the potential barrier of the H-transferCH4, which indicates water molecule inhibits the H-transferOH. Comparison all the four H-transfer modes show that ortho H-transferOH (TS41 and TS78) have lower potential barriers (17.66 kcal/mol for TS41 and 20.11 kcal/mol for TS78) and is thermodynamically more favorable than other H-transfer modes, resulting in the formation of IM35 and IM56. The secondary reaction from the IM35 and IM56 involves two kinds of pathways. Firstly, IM35 and IM56 can undergo C-C bond cleavage and elimination of OH to form dialdehyde (P8 and P18). Secondly, IM35 can be attacked by O2 to form IM39 and HO2. IM39 can be further attacked by O2 and eliminate OH to form carbazolequinone (P9). IM56 can be attacked by O2 to form hydroperoxyl-carbazole-one (P17).

(2) NO addiction reaction

Carbazole-OH-O_2 intermediates have unpaired electrons, which can react with NO to form carbazole-OH-OONO adducts. As shown in Fig. 5, the reactions of NO addition are barrierless and exothermic. Then the carbazole-OH-OONO adducts may undergo NO_2 elimination reactions and produce intermediates IM40, IM51 and IM60. However, these processes are difficult to occur in atmospheric conditions due to the more than 40 kcal/mol potential barriers. Carbazole-OH-OONO adducts can also remove HNO_2 to form hydroxy-carbazole-one (P7 and P12). These elementary reactions are more competitive in atmospheric reaction than NO_2 removal.

Fig. 3 shows the subsequent abstraction reaction of IM5 with O_2. IM6 can undergo an addition reaction with NO and O-ONO bond cleavage to form NO_2 and IM10 adduct, and followed by ring-opening reaction or react with water molecule. Those processes can provide H for unpaired electrons of O to form the product carbazole-ol (P1). The former has high potential barriers (35.21 kcal/mol), which is not easy to occur in the atmosphere, so it is not discussed further. The latter is a barrierless reaction, which is more favorable in the atmospheric environment.

(3) Reactions of bicyclic peroxy radicals

The intramolecular cyclization reaction scheme of carbazole-OH-O_2 adducts IM18, IM19 and IM20 are illustrated in Fig. 6. Four- or five-membered cycle intermediates are formed in the reactions. The formation of five-membered cycle IM32 from the isomerization of IM18 and IM20 is predominating over the others by comparison of the potential barriers and reaction heats. Similarly, the formation of the five-membered cycle IM31 from the isomerization of IM19 is dominated over the formations of IM43-IM45. However, the formation of IM31 from isomerization of IM19 is endothermic by 9.71 kcal/mol with high potential barriers of 34.54 kcal/mol, which indicates that the formation of IM31 is not feasible under common atmospheric conditions. The formations of IM32 from IM18 and IM20 have much lower potential barriers (21.38 and 12.93 kcal/mol) than the formation of IM31 from IM19. Thus, IM32 is a possible bicyclic peroxy radical in the oxidation process of gaseous carbazole and will be further discussed.

Preprints (www.preprints.org) | NOT PEER-REVIEWED | Posted: 29 June 2022 doi:10.20944/preprints202206.0399.v1

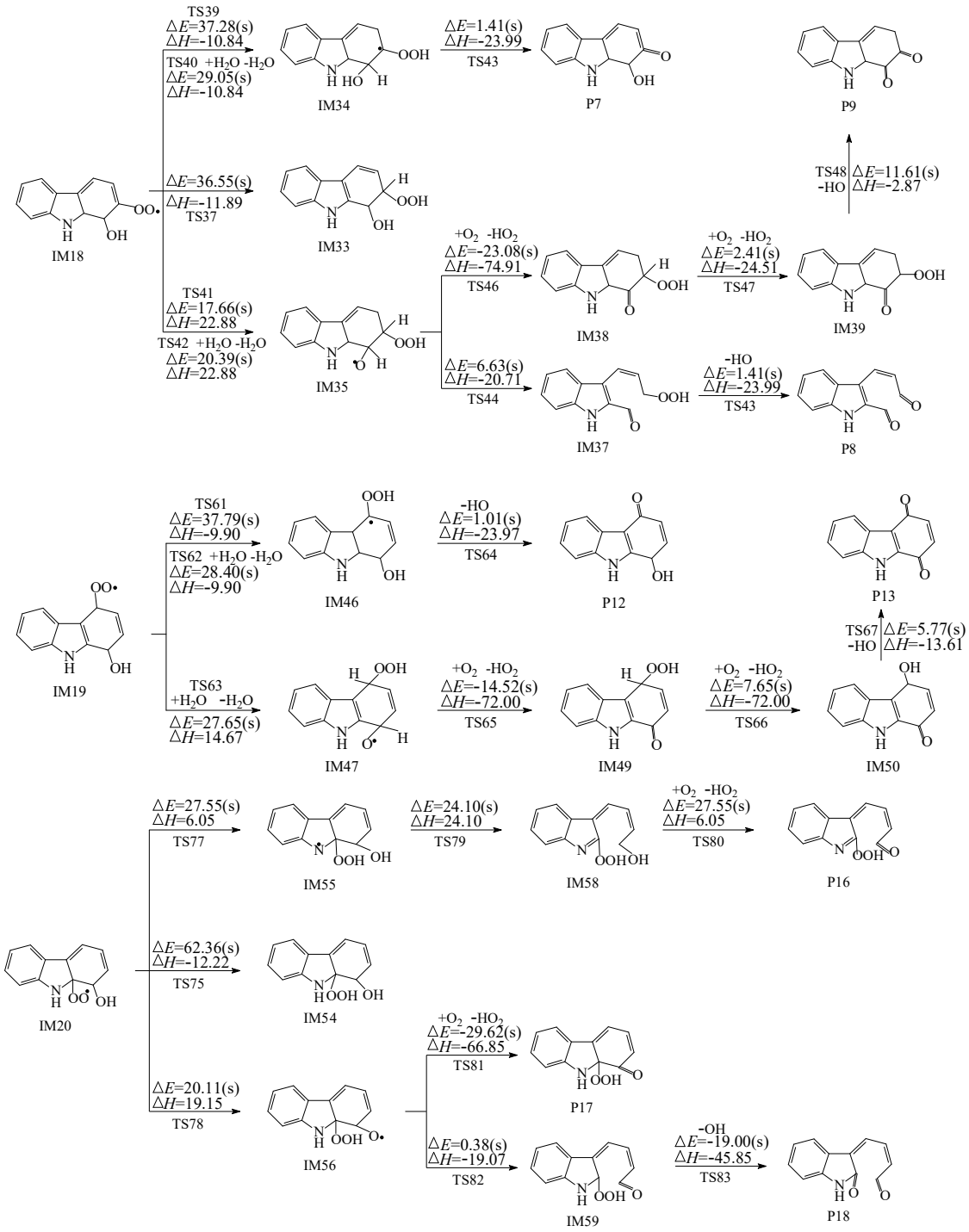

Figure 4. Intramolecular H-transfer reaction of carbazole-OH-O_2 adducts embedded with the potential barrier ΔE (in kcal/mol) and reaction heat ΔH (in kcal/mol, 0 K) with and without H_2O molecular.

As shown in Fig. 7, IM32 can undergo isomerization through O-O bond cleavage or recombine O_2, forming the bicyclic peroxy radical (IM61 and IM62). However, the potential barriers of O-O bond cleavage are 44.50 kcal/mol higher than addition reactions with O_2. Therefore, the cleavage of O-O bonds can possibly compete with the O_2 addition reactions only under the condition of extremely low O_2 concentration. The subsequent reaction of IM61 involves five elementary reactions: addition reaction with NO, NO_2 remove and the cleavage of C-C bond to produce ring-opening radical, the barrierless O-O bond and C-H bond cleavages and the elimination of CHOCHOH radical to form P20.

Preprints (www.preprints.org) | NOT PEER-REVIEWED | Posted: 29 June 2022 doi:10.20944/preprints202206.0399.v1

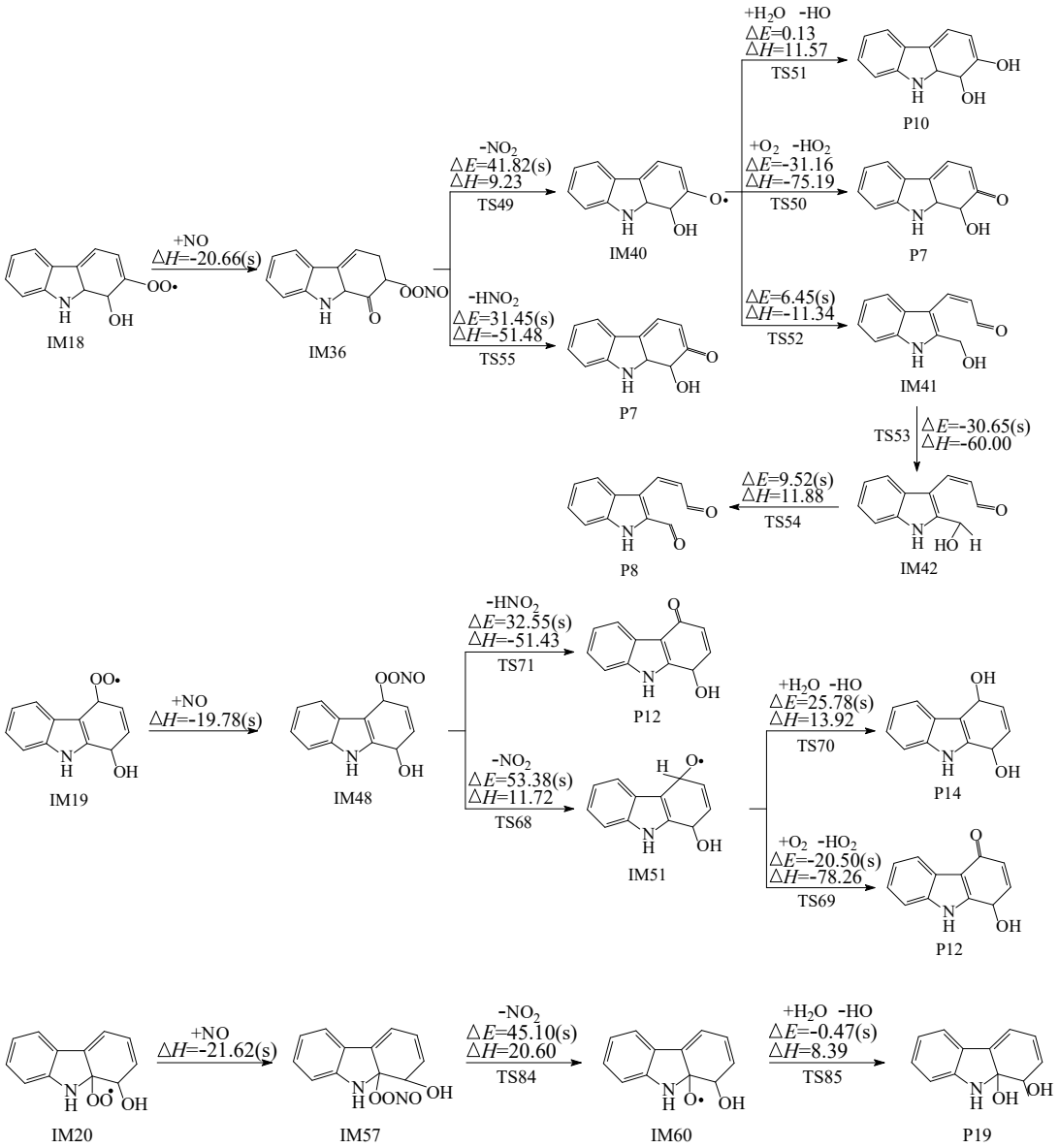

Figure 5. Intramolecular H-transfer reaction of carbazole-OH-O_2 adducts embedded with the potential barrier ΔE (in kcal/mol) and reaction heat ΔH (in kcal/mol, 0 K) with and without H_2O molecular.

As depicted in Fig. 3, IM6 may also combine the C-O bond to form a four- or five-membered ring intermediates IM8 and IM9. However, the formation of IM8 and IM9 are endothermic and need to cross potential barriers of more than 50 kcal/mol. Consequently, IM8 and IM9 are generally unimportant in the atmosphere and will not be discussed further. The intermediate IM5 is not easy to undergo cyclization reaction. Fig. 2 shows the reaction pathways of carbazole-OH adducts (IM12-IM15) with O_2. Firstly, carbazole-OH adducts can react via a simple metathesis mechanism to yield hydroxycarbazoles and HO_2 radical through H abstractions from the C-H bonds. The potential barriers of these hydroxycarbazole formation processes are in the range of −33.66 ~ −29.03 kcal/mol. The processes are strongly exothermic by −68.78 ~ −62.43 kcal/mol. The overall reactions, carbazole + OH + O_2 → hydroxycarbazole + HO_2 have the total potential barriers of −33.33 ~ −27.84 kcal/mol, and are strongly exothermic by −86.02 ~ −83.45 kcal/mol. These indicate that the degradation pathways leading to the hydroxycarbazoles formation are easy to occur under the real atmospheric conditions. A Comparison of the reaction pathways presented in Fig. 2 shows that the formation of 3-hydroxycarbazole (P4) from carbazole + OH + O_2 → hydroxycarbazole + HO_2 has the lowest total potential barriers of −33.33 kcal/mol

Preprints (www.preprints.org) | NOT PEER-REVIEWED | Posted: 29 June 2022 doi:10.20944/preprints202206.0399.v1

and is energetically most favorable relative to the other H abstraction pathways, which means that 3-hydroxycarbazole is the main hydroxycarbazole product.

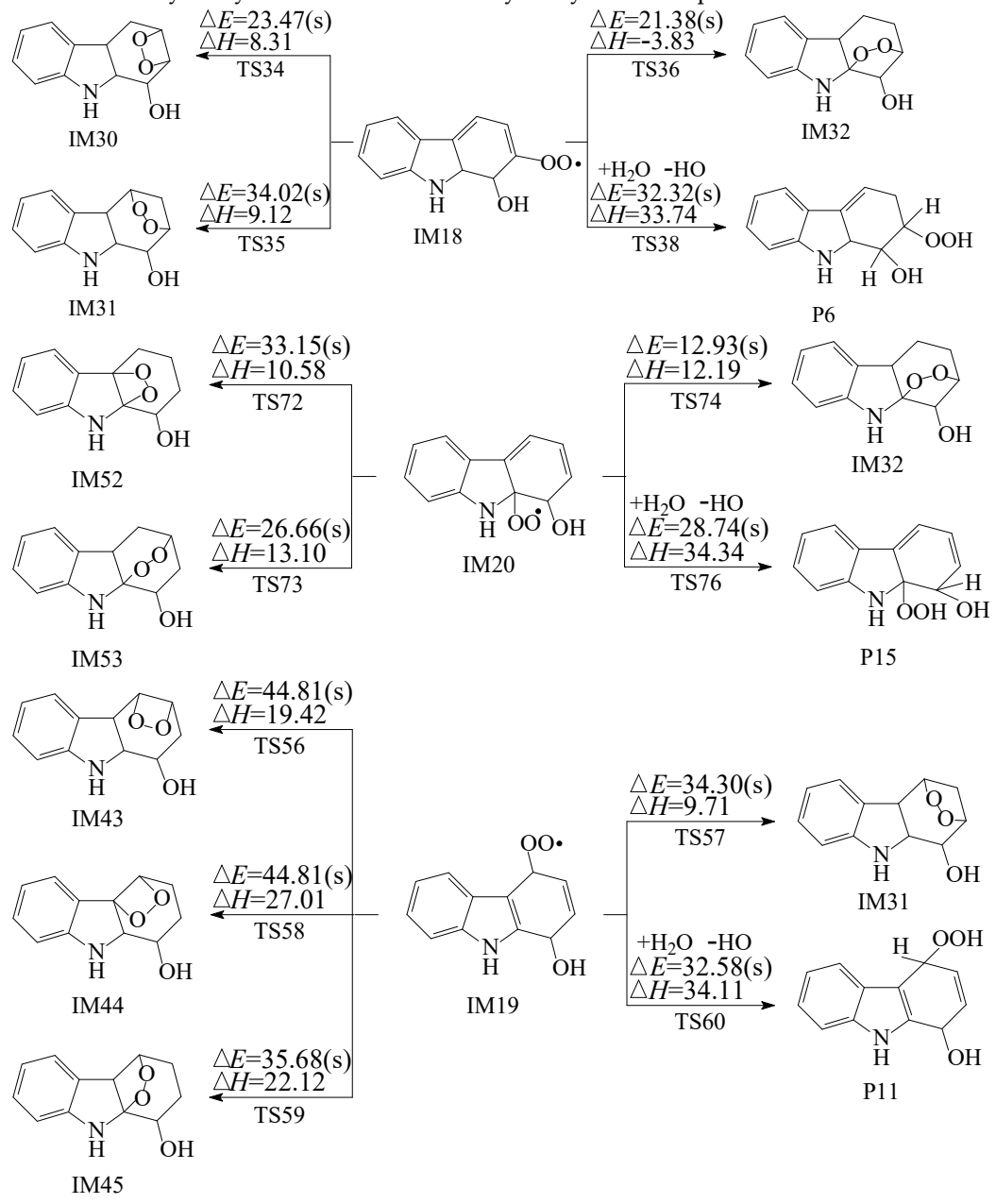

Figure 6. Intramolecular cyclization and H addition reaction scheme of IM18, IM19 and IM20 embedded with the potential barriers ΔE (in kcal/mol) and reaction heats ΔH (in kcal/mol, 0 K) in the presence of H_2O.

Preprints (www.preprints.org) | NOT PEER-REVIEWED | Posted: 29 June 2022 doi:10.20944/preprints202206.0399.v1

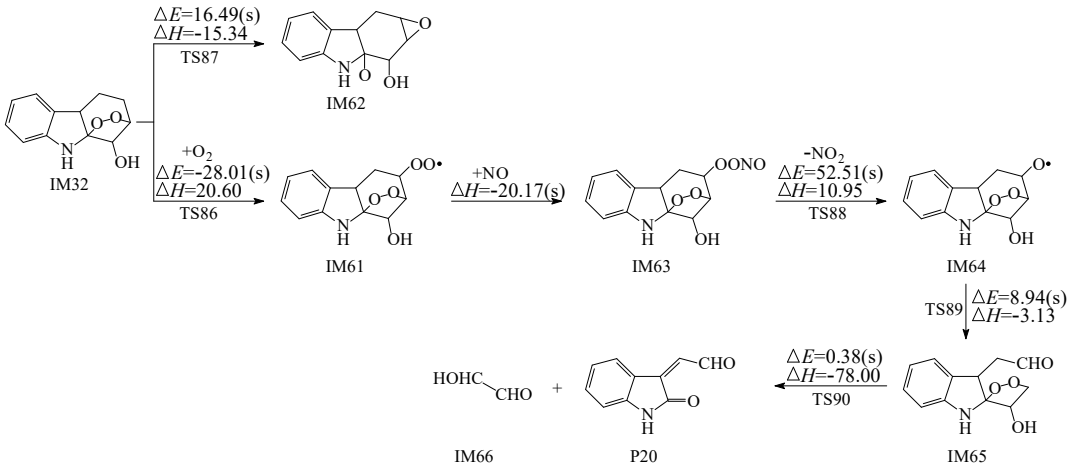

Figure 7. The reaction scheme of IM32 embedded with the potential barriers ΔE (in kcal/mol) and reaction heats ΔH (in kcal/mol, 0 K) in the presence of NO and O_2.

Secondly, carbazole-OH adducts may react with O_2 via H abstractions from the O-H bonds to produce carbazole-epoxides and HO_2 radical. As shown in Fig. 2, the carbazole-epoxide formations from the H abstractions of the O-H bonds have the potential barriers of −16.5 ~ −6.89 kcal/mol, which are higher than the hydroxycarbazole formations from the H abstractions of the C-H bonds. In addition, the carbazole-epoxides formation from the H abstractions of the O-H bonds is exothermic by −25.74 ~ −22.13 kcal/mol, which are less than the hydroxycarbazoles formation from the H abstractions of the C-H bonds. This means that hydroxycarbazole formation is energetically more preferred than carbazole-epoxide formation, e.g. H abstraction from carbazole-OH with O_2 on C-H bond is easier to occur than that on the O-H bond. This may be caused by the differences in bond length and bond energy between the C-H bond and O-H bond in carbazole-OH intermediates. It can be seen from Table S2 that the bond energies of O-H bonds are 40.30 ~ 45.13 kcal/mol higher than those of C-H bonds and the bond lengths are about 0.14 angstrom shorter than the C-H bonds, which indicates that the break of C-H bonds is more favorable than that of O-H bonds.

Thirdly, O_2 can associate with the C atoms in the OH-carbazole adducts with an unpaired electron from two different directions: the anti- or syn-position with respect to the -OH group. Therefore, as depicted in Fig. 2, the O_2 addition reactions in the carbazole-OH adducts can form a series of carbazole-OH-O_2 adducts (namely IM18s/a-IM29s/a, where 's' denotes syn-position and 'a' denotes anti-position O_2 addition). The formation of carbazole-OH-O_2 adducts IM19, IM22, IM25 and IM28 from precursors IM12, IM13, IM14 and IM15 have lower potential barriers and are more exothermic compared to those of other O_2-OH-carbazole isomers. The potential barriers characterizing the formation of syn-position radicals are lower by 0.34 ~ 11.76 kcal/mol than those for the formation of anti-position O_2-OH-carbazole, except for IM18s/a, IM24s/a, IM25s/a and IM26s/a. In most cases, O_2 additions at syn-positions are energetically favored over those at anti-positions. Therefore, the formations of anti-isomers are of minor importance and will not be further discussed. In addition, considering IM12 is the most favored carbazole-OH adducts, the IM12-O_2 adducts (IM18s/a-IM20s/a) will be further discussed.

The scheme of reaction from the H abstraction product of carbazolide anion (IM5) with O_2 is depicted in Fig. 3. As shown in Fig. 3, O_2 may be added to the N atom of IM5 containing unpaired electrons to form OH-carbazole-O_2 adduct IM6. This process is barrierless and strongly exothermic.

Fig. 2 and Fig. 3 show that the O_2 addition on the N atom has higher potential barrier and less heat release than those on the C atoms of the benzene ring, which indicate that the O_2 addition on the N atom is of minor importance than those on the C atoms of the benzene ring.

Preprints (www.preprints.org) | NOT PEER-REVIEWED | Posted: 29 June 2022 doi:10.20944/preprints202206.0399.v1

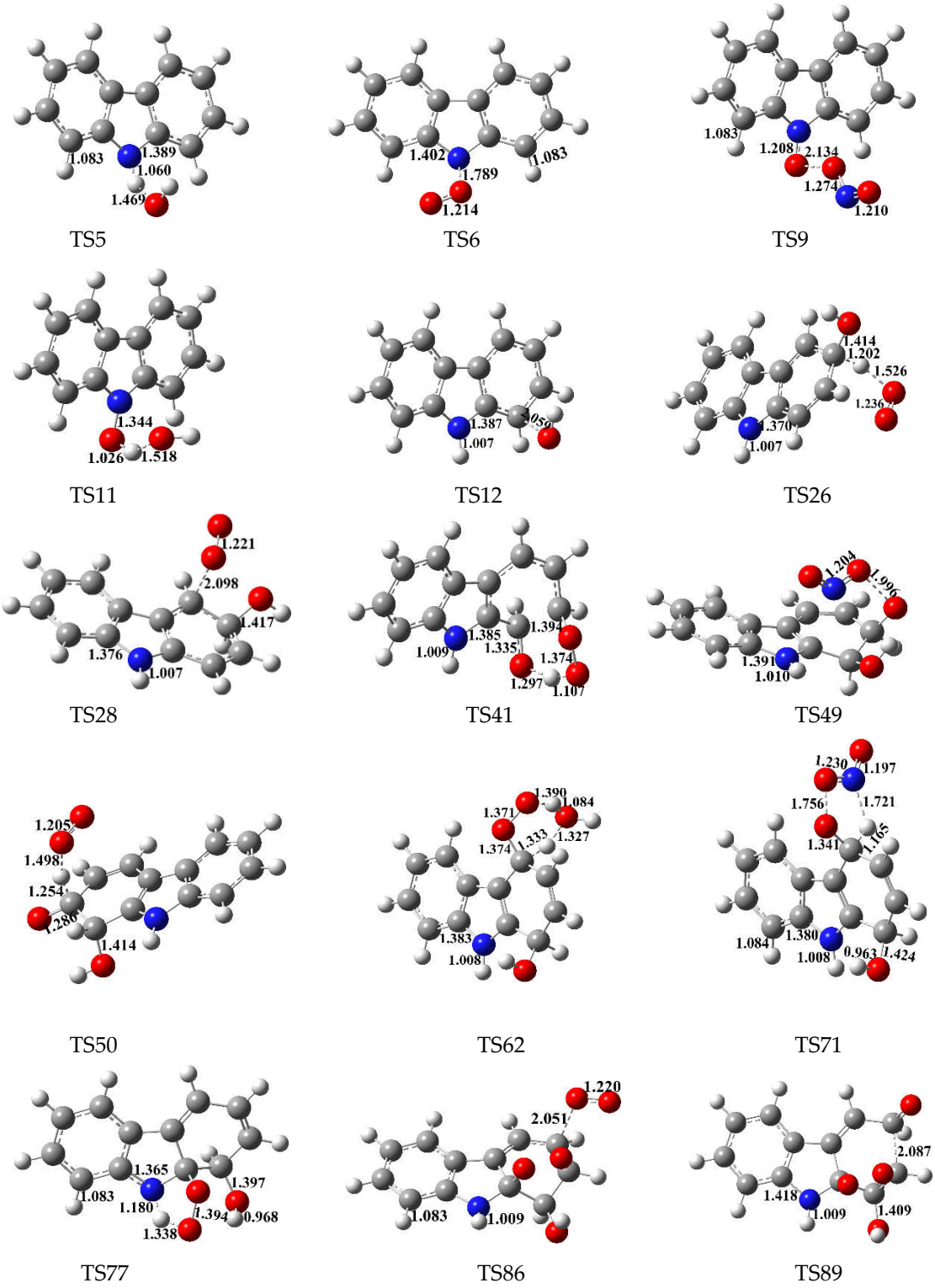

Figure 8. M06-2X/6-311+G(d,p) optimized geometries for typical transition states involved in the degradation of carbazole initiated by OH radical. Distances are in angstroms. Gray sphere, C; Blue sphere, N; Red sphere, O; White sphere, H.

3.3 Rate constant calculations

In order to clarify the transport and atmospheric fate of carbazole, it is of great significance to calculate the accurate rate constants of the elementary reactions involved in the atmospheric oxidation degradation of carbazole. On the basis of energy data obtained at M06-2X/6-311+G(3df,2p)//M06-2X/6-311+G(d,p) level, the rate constants of elementary

Preprints (www.preprints.org) | NOT PEER-REVIEWED | Posted: 29 June 2022 doi:10.20944/preprints202206.0399.v1

reactions were calculated by using RRKM theory [22,23] and MESMER program at 298 K and 1 atm [33]. The previous studies for the PAHs and dioxin-like compound degradation initiated by OH radical have successfully proved the accuracy of RRKM theory to calculate the rate constants for elementary reactions of PAHs and dioxin-like compound degradations [26,41-43]. Thus, it might be inferred that RRKM theory individual rate constants are reasonable in this paper. The calculated rate constants for the elementary reactions in the oxidative degradation of carbazole initiated by OH at 298 K and 1 atm are listed in Table 1.

Table 1. RRKM calculated rate constants (in cm^3 $molecule^{-1}$ s^{-1}) for the elementary reactions involved in the OH-initiated oxidation degradation of carbazole at 298 K and 1 atm.

Reactions	Rate constants
carbazole + OH (k)	8.81×10^{-12}
carbazole + OH (k_{abs})	3.70×10^{-12}
carbazole + OH → IM1 +H_2O (k_1)	1.31×10^{-16}
carbazole + OH → IM2 + H_2O (k_2)	2.03×10^{-16}
carbazole + OH → IM3 + H_2O (k_3)	1.05×10^{-16}
carbazole + OH → IM4 + H_2O (k_4)	2.03×10^{-16}
carbazole + OH → IM5 + H_2O (k_5)	3.70×10^{-12}
carbazole + OH (k_{add})	2.82×10^{-12}
carbazole + OH → IM12 (k_6)	1.23×10^{-12}
carbazole + OH → IM13 (k_7)	2.10×10^{-14}
carbazole + OH → IM14 (k_8)	9.65×10^{-14}
carbazole + OH → IM15 (k_9)	6.09×10^{-14}
carbazole + OH → IM16 (k_{10})	1.01×10^{-15}
carbazole + OH → IM17 (k_{11})	1.61×10^{-16}

In Table 1, the individual rate constants for the H abstraction by OH radical of the C1-H, C2-H, C3-H, C4-H and N-H bonds of carbazole are noted as k_1, k_2, k_3, k_4 and k_5, respectively. In the H abstraction reactions, the H abstraction from the N-H bond has the maximum rate constant of 3.70×10^{-12} cm^3 $molecule^{-1}$ s^{-1}, which is four orders of magnitude higher than those from the C-H bond. The overall rate constant of the OH abstraction reaction is denoted as kabs, $k_{abs} = (k_1 + k_2 + k_3 + k_4) \times 2 + k_5$. The overall rate constant k_{abs} is 3.70×10^{-12} cm^3 $molecule^{-1}$ s^{-1} at 298 K and 1 atm. The individual rate constants for the OH addition to the C1, C2, C3, C4, C10 and C11 bonds of carbazole are noted as k_6, k_7, k_8, k_9, k_{10} and k_{11}, respectively. In the OH addition reactions, the OH addition on C1 has the maximum rate constant of 1.23×10^{-12} cm^3 $molecule^{-1}$ s^{-1}. The overall rate constant of the OH addition reaction is denoted as kadd, $k_{add} = (k_6 + k_7 + k_8 + k_9 + k_{10} + k_{11}) \times 2$. The overall rate constant kadd is 2.82×10^{-12} cm^3 $molecule^{-1}$ s^{-1} at 298 K and 1 atm. The overall rate constant of carbazole with OH is denoted as k, $k = k_{abs} + k_{add}$. The overall rate constant k is 6.52×10^{-12} cm^3 $molecule^{-1}$ s^{-1} at 298 K and 1 atm.

Comparison of the k_5 and k_1, k_5 and k_1 show that the H abstraction from the N-H bond and OH addition on the C1 atom are competitive. This agrees well with the thermal analysis above. The OH addition on C1 and H abstraction on N atom account for 94% of the total reaction rate.

Preprints (www.preprints.org) | NOT PEER-REVIEWED | Posted: 29 June 2022 doi:10.20944/preprints202206.0399.v1

According to the overall rate constants of the reaction of carbazole with OH radical and the average OH concentration in the atmosphere C_{OH} = 9.7 × 10^5 molecule/cm [3,18], from the formula:

$$\tau = \frac{1}{k_{(OH + carbazole)} \times C_{OH}}$$

the atmospheric lifetime of carbazole determined by OH radical is calculated as 43.92 h.

Due to the absence of the available experimental values, it is difficult to make a direct comparison of the calculated rate constants with the experimental data for the reaction of carbazole with OH radical. Therefore, comparison of the lifetime for the reaction of carbazole and OH radical with the literature values of other 5 kinds of NSO-HET compounds and OH radical, and the results are displayed in Table S4. Wallington and Atkinson et al. measured the atmospheric lifetimes of pyrrole and indole with OH were 2.7 h and 2.0 h [28,29], respectively, which were lower than that of carbazole with OH. This may be originated from the different reaction activities and positions of OH attack from benzene ring and hetero cyclopentadiene ring. It can be seen from Table S4 that the lifetime of carbazole with OH is similar to that of dibenzothiophene with OH [27], and longer than those of dibenzofuran/fluorene with OH radical [24,26]. The N/S substitution of NSO-HETs can decrease their reactivity of the reaction with OH radical and increase the lifetime than that from the O/C substitution.

4. Conclusion

In this work, we investigated the atmospheric oxidation of carbazole initiated by OH radical with quantum chemical calculation methods. The mechanism of the formation of main products were determined. In addition, the rate constants and lifetimes for the vital reactions of carbazole degradation by OH radical were evaluated. The rate constants and lifetime of carbazole were compared with those of other five kinds of NSO-HETs. The impact of structure and element substitution of NSO-HETs on the lifetimes were also discussed. This work provides a better understanding of the reactivity of carbazole in the atmospheric environment, the formation of secondary organic aerosols, and the chemical degradation and removal of carbazole in the atmosphere. The main conclusions are as follows:

1. There are four types of reactions for the degradation of carbazole initiated by OH radical: OH additions to "bend" C atoms, OH additions to "benzene ring" C atoms, H abstractions from C-H bonds and the H abstraction from N-H bond. Among them, OH additions to "bend" C atoms and H abstractions from C-H bonds are energetically unfavorable. The best pathway of OH addition reactions is OH addition to C1 atom, which is competitive with the H abstraction from the N-H bond.
2. The primary products of carbazole oxidation by OH radicals in the atmosphere include hydroxycarbazole, dialdehyde, carbazolequinone, carbazole-ol, hydroxy-carbazole-one and hydroperoxyl-carbazole-one.
3. The degradation of carbazole in the atmosphere is significant, for which the rate constant determined by OH radical is 6.52 × 10^{-12} cm^3 $molecule^{-1}$ s^{-1} and the lifetime is 43.92 h. The OH addition on C1 and H abstraction on N atom account for 94% of the total reaction rate. The ranking of the lifetime for the reaction of NSO-HETs with OH is as follows: Pyrrole ≈ Indole < Dibenzofuran ≈ Fluorene < Dibenzothiophene ≈ Carbazole.

Supplementary Materials: The degradation of carbazole in the atmosphere is significant, for which the rate constant determined by OH radical is 6.52 × 10^{-12} cm^3 $molecule^{-1}$ s^{-1} and the lifetime is 43.92 h. The OH addition on C1 and H abstraction on N atom account for 94% of the total reaction rate. The ranking of the lifetime for the reaction of NSO-HETs with OH is as follows: Pyrrole ≈ Indole < Dibenzofuran ≈ Fluorene < Dibenzothiophene ≈ Carbazole.

Acknowledgments: The work was financially supported by National Natural Science Foundation of China (project No. 21876102, 21976107, 22076103), Taishan Scholars (No. ts201712003), the Fundamental Research Funds of Shandong University (project NO. 2016WLJH51, 2017JC033).

Funding: This work was supported by the National Natural Science Foundation of China (project Nos. 21876102, 21976107), the Fundamental Research Funds of Shandong University (No. 2016WLJH51), and the China Postdoctoral Science Foundation funded project (No. 2017M612277, 2017T100493).

Data Availability Statement: The data that support the findings of this study are available from the corresponding author upon reasonable request.

Conflicts of Interest: The authors declare no conflict of interest.

References

1. S. S. Johansen, A. B. Hansen, H. Mosbaek and E. Arvin, Ground Water Monitoring and Remediation, 1997, 17, 106–115.
2. Anonymous and Who, IARC Monographs on the Evaluation of Carcinogenic Risks to Humans, 2008, vol. 97, pp. 9–38.
3. M. Brinkmann, S. Maletz, M. Krauss, K. Bluhm, S. Schiwy, J. Kuckelkorn, A. Tiehm, W. Brack and H. Hollert, Environ Sci Technol, 2014, 48, 5892–5901.
4. A. Eisentraeger, C. Brinkmann, H. Hollert, A. Sagner, A. Tiehm and J. Neuwoehner, Environmental Toxicology and Chemistry, 2008, 27, 1590–1596.
5. F. Esen, Y. Tasdemir and S. S. Cindoruk, Atmospheric Research, 2010, 95, 379–385.
6. J. Roy, A. K. Jana and D. Mal, Tetrahedron, 2012, 68, 6099–6121.
7. S. Ishikawa, Y. Sakazaki, Y. Eguchi, R. Suetomi and E. Nakamura, Chemosphere, 2005, 59, 1343–1353.
8. P. Glarborg, A. D. Jensen and J. E. Johnsson, Progress in Energy and Combustion Science, 2003, 29, 89–113.
9. H. Fromme, W. Mi, T. Lahrz, M. Kraft, B. Aschenbrenner, B. Bruessow, R. Ebinghaus, Z. Xie and L. Fembacher, Sci Total Environ, 2018, 610–611, 412–418.
10. R. Parette, R. McCrindle, K. S. McMahon, M. Pena-Abaurrea, E. Reiner, B. Chittim, N. Riddell, G. Voss, F. L. Dorman and W. N. Pearson, Chemosphere, 2015, 127, 18–26.
11. N. Campbell and B. M. Barclay, Chemical Reviews, 1947, 40, 359–380.
12. Y. M. Aydin, M. Kara, Y. Dumanoglu, M. Odabasi and T. Elbir, Atmospheric Environment, 2014, 97, 271–285.
13. S. Shi, Y. Qu, F. Ma and J. Zhou, Bioresour Technol, 2014, 166, 79–86.
14. P. Xu, B. Yu, F. L. Li, X. F. Cai and C. Q. Ma, Trends in Microbiology, 2006, 14, 398–405.
15. A. L. Larentis, H. C. C. Sampaio, C. C. Carneiro, O. B. Martins and T. L. M. Alves, Brazilian Journal of Chemical Engineering, 2011, 28, 37–44.
16. H. Nojiri and T. Omori, in Pseudomonas: A Model System in Biology, eds. J. L. Ramos and A. Filloux, Springer Netherlands, Dordrecht, 2007, pp. 107–145.
17. S. Heim, J. Schwarzbauer, A. Kronimus, R. Littke, C. Woda and A. Mangini, Organic Geochemistry, 2004, 35, 1409–1425.
18. M. Macleod, M. Scheringer, H. Podey, K. C. Jones and K. Hungerbuehler, Environmental Science & Technology, 2007, 41, 3249–3253.
19. I. J. Keyte, R. M. Harrison and G. Lammel, Chemical Society Reviews, 2013, 42, 9333–9391.
20. M. J. Kurylo and V. L. Orkin, Chemical Reviews, 2003, 103, 5049–5076.
21. S. Wang and D. Chen, Acta Physico-Chimica Sinica, 1995, 11, 1014–1019.
22. D. G. Truhlar, B. C. Garrett and S. J. Klippenstein, Journal of Physical Chemistry, 1996, 100, 12771–12800.
23. O. K. Rice and H. C. Ramsperger, Journal of the American Chemical Society, 1927, 49, 1617–1629.
24. M. Altarawneh, E. M. Kennedy, B. Z. Dlugogorski and J. C. Mackie, Journal of Physical Chemistry A, 2008, 112, 6960–6967.
25. T. V. Mai, H. T. Nguyen and L. K. Huynh, Chemosphere, 2021, 263, 127850.
26. Z. Ding, Y. Yi, Q. Zhang and T. Zhuang, Sci Total Environ, 2019, 669, 920–929.
27. E. S. C. Kwok, R. Atkinson and J. Arey, Polycyclic Aromatic Compounds, 1999, 13, 175–189.
28. T. J. Wallington, International Journal of Chemical Kinetics, 1986, 18, 487-496.
29. R. Atkinson, E. C. Tuazon, J. Arey and S. M. Aschmann, Atmospheric Environment, 1995, 29, 3423–3432.
30. M. J. Frisch, G. W. Trucks, H. B. Schlegel, G. E. Scuseria, M. A. Robb, J. R. Cheeseman, G. Scalmani, V. Barone, B. Mennucci and G. A. Petersson, 2009.
31. Y. Zhao and D. G. Truhlar, Theoretical Chemistry Accounts, 2008, 120, 215–241.
32. K. Fukui, Accounts of Chemical Research, 1981, 14, 363–368.
33. D. R. Glowacki, C. H. Liang, C. Morley, M. J. Pilling and S. H. Robertson, J Phys Chem A, 2012, 116, 9545–9560.
34. R. G. Gilbert and S. C. J. B. S. P. Smith, 1990, 319.
35. S. Y. Lee and B. H. Boo, Journal of Physical Chemistry, 1996, 100, 15073–15078.
36. I. P. Batra, P. S. Bagus, E. Clementi and H. Seki, Theoretica Chimica Acta, 1974, 32, 279–293.
37. K. Lorenz and R. Zellner, Berichte Der Bunsen-Gesellschaft-Physical Chemistry Chemical Physics, 1983, 87, 629–636.
38. R. Ananthula, T. Yamada and P. H. Taylor, Journal of Physical Chemistry A, 2006, 110, 3559–3566.
39. W. Lee, P. S. Stevens and R. A. Hites, Journal of Physical Chemistry A, 2003, 107, 6603–6608.

 doi:10.20944/preprints202206.0399.v1

40. R. Ananthula, T. Yamada and P. H. Taylor, International Journal of Chemical Kinetics, 2007, 39, 629–637.
41. J. Dang and Q. Z. Zhang, Journal of Molecular Modeling, 2018, 24.
42. J. Dang, X. L. Shi, Q. Z. Zhang and W. X. Wang, Science of the Total Environment, 2015, 517, 1–9.
43. N. Zhao, Q. Zhang and W. Wang, Science of the Total Environment, 2016, 563, 1008–1015.